PHYSD2551

ELSEVIER

Physica D 2551 (2000) 1–18

PHYSICA D

www.elsevier.com/locate/physd

Computational macroscopic approximations to the one-dimensional relaxation-time kinetic system for semiconductors

Jose A. Carrillo [a,1], Irene Gamba [a], Chi-Wang Shu [b,*]

[a] *Department of Mathematics, University of Texas at Austin, Austin, TX 78712, USA*
[b] *Division of Applied Mathematics, Brown University, Providence, RI 02912, USA*

Received 23 November 1999; received in revised form 26 June 2000; accepted 28 June 2000
Communicated by C.K.R.T. Jones

Abstract

We study comparisons of deterministic computational methods for one-dimensional relaxation charged transport in submicron channel devices. Our analysis focuses on the appropriate macroscopic approximations under regimes associated to different devices with similar geometries. We show, when taking standard parameters corresponding to Si devices, that the kinetic one-dimensional relaxation model can be approximated by a multi-fluid domain decomposition technique that incorporates classical drift–diffusion equations with corrections in the current. In addition, when considering physical dimensions corresponding to GaAs devices, the technique requires new hydrodynamics that we propose and compute. Our comparison involves detailed computations of local distribution function solution of the kinetic equation, its first three moments compared with the computed fluid variables, and the presentation of all corresponding current–voltage characteristic curves.

PACS: 02.60.Cb; 02.70.Bf; 72.20.Ht; 73.40.c

Keywords: Kinetic theory; Relaxation-time kernel; High field scaling limits; WENO numerical method for conservation laws

1. Introduction

The semi classical Boltzmann equation in the parabolic band approximation is one of the basic equations, and is our starting point for the analysis of charged transport in a semiconductor device. This equation must be coupled to the Poisson equation for determining the self-consistent force field. Though the semi classical Boltzmann–Poisson system is posed in the three-dimensional velocity space, usually the study of simplified devices in one dimension is performed by assuming that the important features of the charge transport are given in the direction parallel to the force field. Therefore considering the low density approximation, taking into account only collisions with background impurities, the collision operator can be approximated by a linear relaxation time operator [10,16]. This equation reads as

* Corresponding author.
E-mail addresses: carri@math.utexas.edu (J.A. Carrillo), gamba@math.utexas.edu (I. Gamba), shu@cfm.brown.edu (C.-W. Shu).
[1] On leave from Departamento de Matemática Aplicada, Universidad de Granada, 18071 Granada, Spain.

0167-2789/00/$ – see front matter
PII: S0167-2789(00)00139-1

$$\frac{\partial f}{\partial t} + v f_x - \frac{e}{m} E(t,x) f_v = \frac{1}{\tau}(M_{\Theta_0}\rho(f) - f), \quad (1.1)$$

$f = f(t,x,v)$ is the density function for an electron at position $x \in [0, L]$ and velocity $v \in \mathbb{R}$ at time $t \geq 0$, where L is the device channel length. The constants e and m represent the unit charge and effective electron mass, respectively. The electric field $E = E(t,x)$ is self-consistently produced by the electrons moving in a fixed ion background with density $C(x)$, called doping profile. E is determined by the Poisson equation

$$\varepsilon_0 \Phi_{xx} = e(\rho(f) - C(x)), \qquad E(t,x) = -\Phi_x, \quad (1.2)$$

where ε_0 is the permittivity of the material and

$$\rho(t,x) = \int_{\mathbb{R}} f(t,x,v)\,\mathrm{d}v,$$
$$j(t,x) = \int_{\mathbb{R}} v f(t,x,v)\,\mathrm{d}v, \quad x \in [0,L], \quad t \geq 0, \quad (1.3)$$

are, respectively, the charge and current densities of the electrons. Here, the relaxation time τ depends on the absolute value of the force field in such a way that the mobility $\mu = (e/m)\tau E$ is linear for small values of $|E|$ with slope μ_0 and has a horizontal asymptote v_d as $|E|$ becomes large. The parameters μ_0 and v_d are known as the bulk mobility and saturation velocity, respectively. M_{Θ_0} is the absolute Maxwellian given by

$$M_{\Theta_0} = (2\pi\Theta_0)^{-1/2} \exp\left(-\frac{v^2}{2\Theta_0}\right),$$

where Θ_0 is the lattice temperature, that is, $\Theta_0 = (k_\mathrm{B}/m)T_0$ with the Boltzmann constant k_B and the lattice temperature T_0 in Kelvin.

The aim of the numerical study we develop in this paper is to show that different scalings appear in simple channel corresponding to dimensions for Si and GaAs one-dimensional semiconductor device models, and in a sense, to propose a domain decomposition based on local dimensionless parameters.

The change of these local dimensionless parameters reflects a delicate interplay between the magnitudes of doping drop per channel length, the applied bias, the bulk mobility, the saturation velocity and the constitutive form used for the relaxation time.

We consider an n^+–n–n^+ device as benchmark for our simulations as it has been done in many works in the literature [1,2,6,11,13,15] and references therein. We study the improvement on the current–voltage curves given by the different approximations in each case choosing the correct hydrodynamic system depending on the dominant regime. With this aim, Section 2 is devoted to review the different scalings for the system (1.1) and (1.2) and their hydrodynamics approximations. We review the different order of approximations for the distribution function and we introduce a new hydrodynamic model for the ballistic scaling. In Section 3 we describe the numerical method used in this paper for the kinetic system and its hydrodynamics approximations. We also explain how we compute the different first order approximation distribution functions. Also, since typically the regimes are different throughout the device, we use a domain decomposition at the hydrodynamical level whose numerical procedure is detailed in Section 3. Sections 4 and 5 describe the results for typical one-dimensional semiconductor devices of Si and GaAs, respectively. As expected, we show that the scalings for these two devices are different in the channel and we compute different hydrodynamical approximations for them. We show that in this way the current–voltage curves are improved with respect to the standard drift–diffusion-Poisson system and other hydrodynamic systems proposed in the literature, when compared with the corresponding computations of the current–voltage curves for the kinetic Poisson model.

2. Scalings and hydrodynamical regimes

Let L be the characteristic length of the device and ρ_0 be the average value of the doping profile $C(x)$. We consider four different time scales or, equivalently, characteristic velocities: $\Theta_0^{1/2}$ is the reference magnitude for the *thermal velocity*. With τ_0 we denote a reference value for the relaxation time $\tau(x)$ and then, for the *relaxation velocity* L/τ_0. Let $[\Phi]$ be the potential drop ("forward bias") applied to the contacts of the device of length L. Then the reference magnitude

for the *drift velocity* $-\tau(e/m)E$ is given by

$$U_0 = \tau_0 \frac{e}{m} E_0 = \tau_0 \frac{e}{m} \frac{[\Phi]}{L},$$

and the reference value for the *ballistic velocity* is

$$B_0 = \sqrt{2\frac{e}{m}[\Phi]}.$$

The name of ballistic velocity comes from the fact that for high fields there will be some particles not undergoing any collisions in the channel for which their trajectories follow the paths of the ordinary differential system conserving energy, that is,

$$m\frac{|v|^2}{2} - e\Phi(x) = \text{const.}$$

This interpretation of the ballistic speed makes sense only in the stationary case. With the above characteristic speeds we introduce new, non-dimensional variables as

$$\begin{aligned} &x = L\hat{x}, \qquad v = V_1\hat{v}, \qquad t = \frac{L}{V_2}\hat{t}, \\ &\tau(x) = \tau_0\hat{\tau}(\hat{x}), \qquad C(x) = \rho_0\hat{C}(\hat{x}), \\ &\Phi(t,x) = [\Phi]\hat{\Phi}(\hat{t},\hat{x}), \end{aligned} \tag{2.1}$$

and for the density function $\hat{f}(\hat{t},\hat{x},\hat{v})$ we shall consider:

$$f(t,x,v) = \frac{\rho_0}{V_3}\hat{f}(\hat{t},\hat{x},\hat{v}). \tag{2.2}$$

Here, V_1, V_2 and V_3 are the characteristic values for the velocity that we will choose among the thermal, relaxation, drift or ballistic velocity to obtain each of the relevant scalings.

Let us define the following dimensionless parameters:

$$\eta = \frac{U_0}{\Theta_0^{1/2}}, \qquad \epsilon = \frac{\tau_0\Theta_0^{1/2}}{L}, \tag{2.3}$$

$$\alpha = \frac{U_0}{B_0} = \frac{\tau_0 B_0}{2L}, \qquad \beta = \frac{\Theta_0^{1/2}}{B_0}, \tag{2.4}$$

$$\gamma = \frac{\rho_0 e L^2}{\varepsilon_0[\Phi]}. \tag{2.5}$$

Let us consider the following different scalings of Eq. (1.1). We indicate for each scaling the characteristic values of the velocities V_1, V_2 and V_3 and the resulting dimensionless equation after dropping the hats.

1. *Low field scaling* (LFS): $V_1 = V_3 = \Theta_0^{1/2}$, $V_2 = U_0$ and $\eta \simeq \epsilon \to 0$.

$$\epsilon\frac{\partial f}{\partial t} + vf_x - E(t,x)f_v = \frac{1}{\epsilon}\frac{1}{\tau}(M_1\rho(f) - f), \tag{2.6}$$

2. *Drift–collision balance scaling* (DCBS): $V_1 = \Theta_0^{1/2}$, $V_2 = V_3 = U_0$, $\eta = 0(1)$ and $\epsilon \to 0$.

$$\eta\frac{\partial f}{\partial t} + vf_x - \frac{\eta}{\epsilon}E(t,x)f_v = \frac{1}{\epsilon}\frac{1}{\tau}(M_1\rho(f) - f), \tag{2.7}$$

3. *Ballistic scaling* (BS): $V_1 = V_2 = V_3 = B_0$, $\alpha = 0(1)$ and $\beta \to 0$.

$$\frac{\partial f}{\partial t} + vf_x - \frac{1}{2}E(t,x)f_v = \frac{1}{2\alpha}\frac{1}{\tau}(M_{\beta^2}\rho(f) - f). \tag{2.8}$$

All of them are coupled to the dimensionless Poisson equation given by

$$\Phi_{xx} = \gamma(\rho(f) - C(x)) \tag{2.9}$$

for the LFS and the BS or

$$\Phi_{xx} = \gamma(\eta^{-1}\rho(f) - C(x)) \tag{2.10}$$

for the DCBS.

Both the LFS and the DCBS admit a Hilbert or a Chapman–Enskog expansion procedure that calculates the moment equations and the corresponding hydrodynamics approximations. We will indicate the resulting hydrodynamic system together with the first order approximation for the density function which is obtained in each scaling above.

The LFS limit ($\epsilon \to 0$, $\eta \simeq \epsilon$) means that the collisions are dominant in this scale (the drift speed is much smaller than the thermal speed) and then we take the limit for small mean free path. This is the reason why this scaling is called low field scaling. The Hilbert expansion for the LFS gives the classical standard drift–diffusion-Poisson (DDP) system (see [16]). They read in dimensionalized form

$$\rho_t + \partial_x(-\tau\Theta_0\rho_x - \mu\rho E) = 0, \tag{2.11}$$

$$E = -\Phi_x, \qquad \varepsilon_0\Phi_{xx} = e(\rho(f) - C(x)), \tag{2.12}$$

where $\mu = e\tau(x)/m$. In this case the distribution solution $f(t, x, v)$ of the kinetic system (1.1) and (1.2) is approximated by

$$f(t, x, v) = \rho(t, x)M_{\Theta_0}(v) + \mathrm{o}(\epsilon).$$

The DCBS limit ($\eta = 0(1)$ and $\epsilon \to 0$) means that the collisions continue to be dominant but the force field is higher and now the drift speed is of the order of the thermal speed. In this sense this scaling appears for higher potential drops than the LFS. The following equations are the corresponding ones to the DCBS as presented in [9,10] for the lowest moments. The corresponding augmented–drift–diffusion-Poisson (ADDP) system in its dimensionalized form reads

$$\rho_t + \partial_x(j_{\mathrm{hyp}} + j_{\mathrm{vis}}) = 0, \tag{2.13}$$

$$j_{\mathrm{hyp}} = -\mu\rho E + \tau\mu\left(\frac{e}{\varepsilon_0}\right)\rho(-\mu\rho E + \omega), \tag{2.14}$$

$$j_{\mathrm{vis}} = -\tau[\rho(\Theta_0 + 2\mu^2E^2)]_x + \tau\mu E(\mu\rho E)_x, \tag{2.15}$$

$$E = -\Phi_x, \qquad \varepsilon_0\Phi_{xx} = e(\rho(f) - C(x)). \tag{2.16}$$

The constant ω is fixed as

$$\omega = (\mu\rho E)|_{x=x_\omega}, \tag{2.17}$$

where x_ω is some point in the computational region. The total current $j(t, x)$ is approximated by $j_{\mathrm{hyp}} + j_{\mathrm{vis}}$. We refer to [10] and the references therein for a deeper discussion of this system and the role of ω.

In the case of the DCBS regime, the density $\rho(t, x)$ and current $j(t, x)$ that solve the ADDP system (2.13)–(2.17) are asymptotic approximations of the first and second moments of $f(t, x, v)$ solution of the kinetic system (1.1) and (1.2), respectively. In particular

$$f(t, x, v) = \rho(t, x)P_{-\mu E,\Theta_0} + \mathrm{o}(\epsilon),$$

where P_{ξ,Θ_0} is the probability density solving the equation

$$\xi\,\partial_v P_{\xi,\Theta_0} = -P_{\xi,\Theta_0} + M_{\Theta_0} \tag{2.18}$$

for $\xi \in \mathbb{R}$. The distribution P_{ξ,Θ_0} has an explicit formula, given in (3.1) and (3.2), making all its moments computable.

The BS limit ($\alpha = 0(1)$ and $\beta \to 0$) means that the potential is significantly higher than in previous cases and the drift speed is of the order of the ballistic speed and much larger than the thermal speed. With this picture of the three scalings the DCBS is an intermediate scaling between the LFS and the BS. The case of the ballistic regime is quite different, since no asymptotic expansion of the Hilbert or Chapman–Enskog type are possible. In this case we propose a new hydrodynamic closure based on numerical studies of the solution of the kinetic system (1.1) and (1.2) under data that corresponds to ballistic regime in a region of the device.

Once we have studied the different scalings and their first order terms for the distribution function, we attempt to develop a hydrodynamical system for calculating the solution in a computationally faster way. This has been accomplished in the low field scaling (LFS) and DCBS, by introducing the DDP and ADDP systems, respectively, in which only the evolution of the density of particles is considered.

For the ballistic scaling regime we shall use a moment closure method. This method, originally developed for the Boltzmann equation in the theory of gases (Grad's moment's method [12]) and extended, by Bloktejaer [6], Baccarani and Woderman [2] to charged transport in semiconductor structures, is based on the study of equations for the evolution of more moments in velocity, density, current and energy and to perform a closure for the unknown moments in the equation of the energy. In [2] the authors propose an ad hoc closure imposing a Fourier type law (Franz–Wiederman Law) to account for the heat flux and need to impose many free parameters. For a recent review of the numerical methods for the kinetic and hydrodynamic systems we refer to [17].

Recently, with the aid of Monte Carlo simulations, closure modifications were proposed by Anile et al. [1] by calibrating free parameters and using the entropy minimization method, as an alternative way to macroscopic hydrodynamic approximations. The resulting system has the modified flux in the energy equation satisfying the Onsager reciprocity relations that have

not been accounted for in the previous models. Again these closures seem to produce good results for relatively moderate fields such as that in Si channel devices, but the relative errors are too large for shorter channels or devices with higher bulk mobility and saturation speeds.

Here, we propose to derive a hydrodynamic closure in the ballistic scaling. This problem was previously treated by Shur and Eastman [19] by introducing a closure based on the assumption that the distribution function is a Dirac delta point mass concentrated at the local ballistic speed. Such an assumption neglects any collision effect which is widely observed with Monte Carlo and deterministic methods (for example these presented in this paper). Also Ben Abdallah et al. [4,5] proposed a Child–Langmuir asymptotics for the relaxation kinetic equation with the shortcomings that it can only be worked out in the stationary case and for zero temperature. They proved that the distribution function splits into a bounded part and ballistic shifted point mass distribution. Although this is a better approximation than the model in [19] for a stationary state, it does not take into account positive temperature and the effect of the collisions only appears in the bounded part of the distribution function. Nevertheless, in both cases computations of IV curves show a remarkable improvement in the approximation of the kinetic IV curves with respect to drift–diffusion or the (BBW) hydrodynamic system under ballistic regimes.

Our present deterministic time-dependent computations under the ballistic scaling regime show that, after reaching stationary states, double hump distributions are observed making the approximation of [4,5] a better one than that in [19]; however the second spike, localized at the ballistic local speed is not nearly a point mass distribution as assumed in [4,5,19].

Therefore, based on our numerical result, we propose a new system of hydrodynamic equations, valid only in the ballistic scaling regime, that can be thought as an improvement of the Shur–Eastman model based on the splitting of the distribution function studied by Ben Abdallah et al.

The scaling parameters will enter only in the way we choose the closure ansatz for the energy flux, i.e. the third moment in velocity. Let us consider as usual the density, current and energy for the density function f as

$$\rho(t,x) = \int_{\mathbb{R}} f(t,x,v)\,\mathrm{d}v,$$

$$j(t,x) = \rho u(t,x) = \int_{\mathbb{R}} v f(t,x,v)\,\mathrm{d}v,$$

$$\rho W(t,x) = \frac{1}{2}\int_{\mathbb{R}} v^2 f(t,x,v)\,\mathrm{d}v,$$

$$\rho S(t,x) = \int_{\mathbb{R}} v^3 f(t,x,v)\,\mathrm{d}v.$$

Multiplying Eq. (1.1) by 1, v, v^2 and integrating it in v, we find the standard equations

$$\rho_t + (\rho u)_x = 0, \tag{2.19}$$

$$(\rho u)_t + (\rho u^2 + p)_x = -\frac{e}{m}E\rho - \frac{1}{\tau}\rho u, \tag{2.20}$$

$$(\rho W)_t + \left(\frac{1}{2}\rho S\right)_x = -\frac{e}{m}E\rho u - \frac{1}{\tau}\rho(W - W_0), \tag{2.21}$$

where

$$\mathcal{E} = \rho W = \tfrac{1}{2}\rho\Theta + \tfrac{1}{2}\rho u^2 = \tfrac{1}{2}p + \tfrac{1}{2}\rho u^2$$

defines the energy per unit mass $\mathcal{E}$, the local temperature $\Theta = (k_B/m)T$ and the pressure $p = \rho\Theta$ and $W_0 = \frac{1}{2}\Theta_0$.

The new features appear as a consequence of the way the third moment is computed in terms of the first three moments in v. Our closure assumption is to assume that f is not far from being a convex combination of the first order expansion for the DCBS and a shifted Maxwellian with mean velocity given by the ballistic velocity and fixed variance $\Theta_1 = k\Theta_0$, $0 < k < 1$ being a fraction of the lattice temperature. In addition the choice of the convex combination parameter ν and the fraction of the lattice temperature Θ_1 must satisfy the condition imposed on the closure assumption that the first three moments of the closure and the solution must be equal. This delivers a relation between ν, Θ, Θ_0 and Θ_1.

The motivation for this closure arises from our numerical results (Figs. 6 and 7) in which we see a

thickening of the tail of f in a very similar shape as $P_{-\mu E,\Theta_0}$ with the temperature lattice and a peak moving approximately with the ballistic velocity and an unknown variance.

Then, for the closure selection we consider our scaling assumptions. Assume the ballistic regime holds in the channel, then $\alpha = 0(1)$ and $\beta \to 0$ and thus, the drift velocity $-\mu E$ is of the same order as the ballistic velocity B, while B is of the order of the mean velocity u.

Therefore, we assume that $u \simeq B$ and $u \simeq -\mu E$. With this scaling assumption we have

$$f \simeq f_0 = \rho(\nu P_{u,\Theta_0} + (1-\nu)M_{\Theta_1}(v-u)). \quad (2.22)$$

We find a relation between ν and Θ_1 in terms of the local temperature by imposing that f_0 has the first three moments equal to f, that is,

$$\int_{\mathbb{R}} (v-u)^2 f_0 \,\mathrm{d}v = \nu u^2 + \nu\Theta_0 + (1-\nu)\Theta_1 = \Theta = \int_{\mathbb{R}} (v-u)^2 f \,\mathrm{d}v. \quad (2.23)$$

Next, in order to compute the closure equation we approximate the energy flux $\frac{1}{2}\rho S$ by computing the third moment of f_0 in (2.22) and replacing it in (2.21). Thus, we deduce

$$\rho S = \int_{\mathbb{R}} v^3 f(t,x,v)\,\mathrm{d}v = \int_{\mathbb{R}} v(v-u)^2 f(t,x,v)\,\mathrm{d}v + 2\rho uW + up$$

with

$$\int_{\mathbb{R}} v(v-u)^2 f(t,x,v)\,\mathrm{d}v \simeq \int_{\mathbb{R}} v(v-u)^2 f_0(t,x,v)\,\mathrm{d}v,$$

and computing the moments of P_{u,Θ_0} and $M_{\Theta_1}(v-u)$ we find

$$\int_{\mathbb{R}} v(v-u)^2 f_0(t,x,v)\,\mathrm{d}v = \nu\rho u\Theta_0 + 3\nu\rho u^3 + (1-\nu)\rho u\Theta_1.$$

Then,

$$\tfrac{1}{2}\rho S = \rho uW + \tfrac{1}{2}pu + \tfrac{1}{2}\nu\rho u\Theta_0 + \tfrac{3}{2}\nu\rho u^3 + \tfrac{1}{2}(1-\nu)\rho u\Theta_1.$$

Using the relation (2.23) between Θ_1, Θ and Θ_0, replacing $(1-\nu)\Theta_1 u$ by $\Theta u - \nu\Theta_0 u - \nu u^3$ in the last term, we have that the third hydrodynamic equation (2.21) reads as

$$(\rho W)_t + (\rho uW + pu + \nu\rho u^3)_x = -\frac{e}{m}E\rho u - \frac{1}{\tau}\rho(W - W_0), \quad (2.24)$$

where ν should satisfy condition (2.23) for Θ_1 chosen.

Thus, we can use the system of conservation laws (BHD)=(2.19), (2.20) and (2.24) to compute the macroscopic quantities in the ballistic regime on the channel.

In general, the BHD system depends on the chosen value for Θ_1. As previously stated the closure becomes a better approximation for Θ_1 chosen as a fraction of the lattice temperature Θ_0. This is motivated by the kinetic numerical results in Section 5 (Figs. 6 and 7). In this case ν is a function of u and Θ through the relation (2.23). The resulting system will be denoted by BHDT indicating we use a ballistic hydrodynamic system with given temperature for the ballistic peak.

If we take $\Theta_1 = \Theta$ and $\alpha = 1$, we find $\nu = 0$. We will denote this hydrodynamic system by the ballistic hydrodynamic system with $\nu = 0$ (BHD_0) corresponding to pure ballistic transport $\nu = 0$ in (2.22). Although there is no apparent way to justify that such a choice is a good one for a process with collisions, it is quite remarkable that the computation of the corresponding hydro model produces IV curves that approach the kinetic IV curves with quite good accuracy (Fig. 10), even with respect to the choice of other parameters. This effect might explain why many approximations of ballistic regimes compute just Vlasov–Poisson systems, or their hydrodynamic approximations, and then add *boundary effects* that account for the transition from the ballistic to low field scales.

Computed comparisons of IV curves for the BHD_0 and the BHDT models (Fig. 10) show that this regime is a very good approximation for voltages between 0.5–2 V for the GaAs channel.

The case $\Theta_1 = 0$ was studied in [4,5] obtaining that the steady distribution function was the sum of

two distribution functions, one of them being the delta Dirac function localized at the local ballistic velocity and the other one a distribution function which takes into account the collisions in the channel. In a sense our closure may be interpreted as a dynamical approximation that takes into account this splitting of the distribution function as well. The thickness of the tail and of the ballistic peak may be treated more rigorously by a more sophisticated closure procedure in which all the parameters involved are obtained from the solution of a much more involved hydrodynamic-type system. The generalization to three dimensions in velocity for the relaxation Boltzmann–Poisson can be done by assuming that the distribution function is basically P_{u,Θ_0} in the direction of the force field times a Maxwellian distribution in the perpendicular velocities. This approach is currently under investigation.

We must add that at the present stage, the relation (2.23) involves one free parameter that must be chosen. These may appear as a disadvantage, but we point out that all other alternatives, presented so far as approximations to ballistic regimes, also require the selection of a free parameter, as shown above in the Shur–Eastman model (i.e. for the choice of $\eta = 0$ and $\Theta_1 = \Theta = 0$) or the Child–Langmuir asymptotics which is an stationary approximation of the choice $\eta = 1$, $\Theta = 0$ in (2.23) plus a Dirac delta distribution localized at the local ballistic speed.

Let us remark that the ballistic speed and thus, the ballistic shifted Maxwellian are only physically meaningful for the stationary solution. Therefore, the proposed BHD systems may not be good approximations for the transient behavior of the kinetic solution in such inhomogeneous domain. Though our computations are time-dependent in both the kinetic and the BHD cases, the presented comparison of both outputs are in the stationary limit.

Before finishing this section, we have to clarify the boundary conditions for the several systems introduced. The one-dimensional Boltzmann–Poisson kinetic equation will be supplemented by the boundary conditions

$$f(t, 0, v) = C(0)M_{\Theta_0}(v) \quad \text{for} \quad v > 0,$$
$$f(t, L, v) = C(L)M_{\Theta_0}(v) \quad \text{for} \quad v < 0.$$

The DDP system is considered with Dirichlet boundary conditions for the density

$$\rho(t, 0) = C(0), \qquad \rho(t, L) = C(L).$$

The ADDP system will be computed only in the channel with Dirichlet boundary conditions for the density obtained by a domain decomposition method which will be explained below. Finally, all the hydrodynamic systems will be supplemented by Dirichlet boundary conditions for the density and the temperature and computed only in the channel. The value of the temperature would be chosen to be the lattice temperature while the value of the density will be obtained from the DDP system steady results. All models are coupled to the Poisson equation with the boundary conditions $\Phi(t, 0) = 0$, $\Phi(t, L) = V_{\text{bias}}$.

Finally, we would like to mention that we use the local dimensionless parameters computed from the Boltzmann–Poisson equation as indicators to decide which asymptotic limit holds in the channel. Ideally, a theoretical study is needed to ensure a priori which asymptotics (LFS, DCBS, BHD) should be implemented, depending on the physical parameters of the model under consideration. From our computational experiment it is clear that the range of values of the dimensionless parameters throughout the channel depends on the balance between relationships involving the effective mass, channel length, potential drop, saturation velocity and bulk mobility, as well as the choice of the constitutive form of the relaxation as a function of the force field. Such an analysis has to be performed and will be part of a future project.

3. Numerical method

We use the finite difference ENO schemes developed in [18] and the weighted ENO (WENO) schemes developed in [14]. Time discretization is via the TVD (total-variation-diminishing) third order explicit Runge–Kutta method in [18]. Steady state is achieved by asymptotic time marching with initial conditions obtained from a continuation in *vbias*. These schemes are designed for hyperbolic conservation laws or other convection dominated problems.

They are especially effective for problems containing either discontinuous solutions or solutions with sharp gradients. The guiding principle is an adaptive local choice of a stencil (ENO), or use of a nonlinear convex combination of contributions from local stencils (WENO), so that contributions from stencils containing a possible discontinuity or other unpleasant features (e.g., a high gradient) are either completely avoided (ENO) or are assigned a nearly zero weight (WENO). In doing this, uniform high order accuracy can be achieved without introducing any oscillations near discontinuities or sharp gradient regions. The high order accuracy of these algorithms allows us to use relatively coarse grids and still get very accurate results. The algorithms are extremely stable and robust in all the numerical simulations.

We make a few remarks about the computation of the probability density function from (2.18):

$$P_{\xi,\Theta_0}(v) = \frac{1}{\xi}\exp\left(\frac{\Theta_0}{2\xi^2} - \frac{v}{\xi}\right) \frac{1}{2}\mathrm{erfc}\left(-\frac{1}{\sqrt{2\Theta_0}}\left(v - \frac{\Theta_0}{\xi}\right)\right), \quad \xi > 0, \tag{3.1}$$

where

$$\mathrm{erfc}(x) = \frac{2}{\sqrt{\pi}}\int_x^\infty \mathrm{e}^{-t^2}\,\mathrm{d}t. \tag{3.2}$$

For $\xi < 0$ we use

$$P_{\xi,\Theta_0}(v) = P_{-\xi,\Theta_0}(-v). \tag{3.3}$$

The function erfc as defined by (3.2) is an intrinsic function in FORTRAN. However, the evaluation of $P_{\xi,\Theta_0}(v)$ in (3.1), when the argument of erfc is too large,

$$x = -\frac{1}{\sqrt{2\Theta_0}}\left(v - \frac{\Theta_0}{\xi}\right) > 6, \tag{3.4}$$

has numerical difficulties. We thus use the asymptotic expansion of erfc for large x,

$$\mathrm{erfc}(x) = \frac{2}{\sqrt{\pi}}\frac{\mathrm{e}^{-x^2}}{2x}\sum_{m=0}^{\infty}\frac{(-1)^m(2m)!}{m!(2x)^{2m}}, \tag{3.5}$$

to obtain the following equivalent formula for $P_{\xi,\Theta_0}(v)$,

$$P_{\xi,\Theta_0}(v) = \frac{1}{\xi}\mathrm{e}^{-v^2/2\Theta_0}\frac{1}{\sqrt{\pi}}\frac{1}{2x}\sum_{m=0}^{\infty}\frac{(-1)^m(2m)!}{m!(2x)^{2m}} \tag{3.6}$$

with x given by (3.4). The summation is performed to a term which is less than 10^{-15}. We have verified that (3.1) and (3.6) give identical results when both are stable.

Finally, we comment on the procedures used in the domain decomposition. The interval $[0, L]$ is broken into three subintervals: $[0, A]$, $[A, B]$ and $[B, L]$. The exact methods to determine A and B will be discussed in the next two sections. A and B could

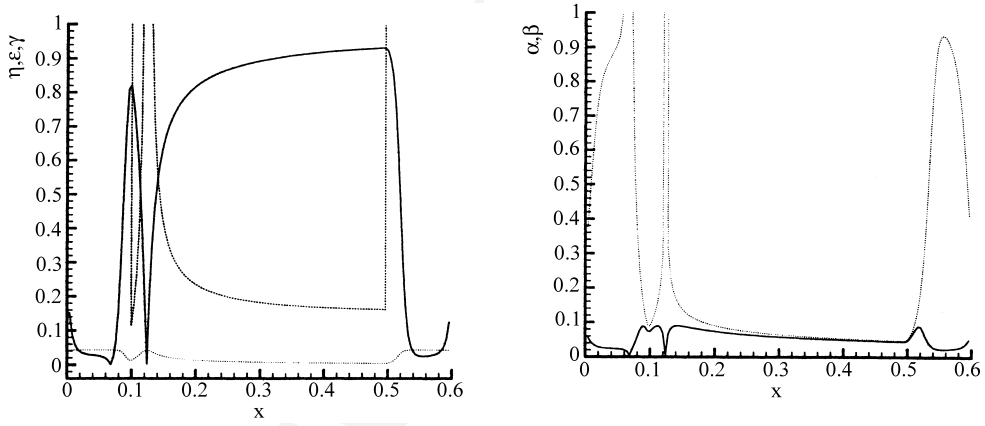

Fig. 1. Local non-dimensional parameters for the Si device, calculated with $E(x)$ from the kinetic simulation results. Left figure: solid line, $\eta(x)$; dotted line, $\varepsilon(x)$; dashed line, $\gamma(x)$. Right figure: solid line, $\alpha(x)$; dotted line, $\beta(x)$.

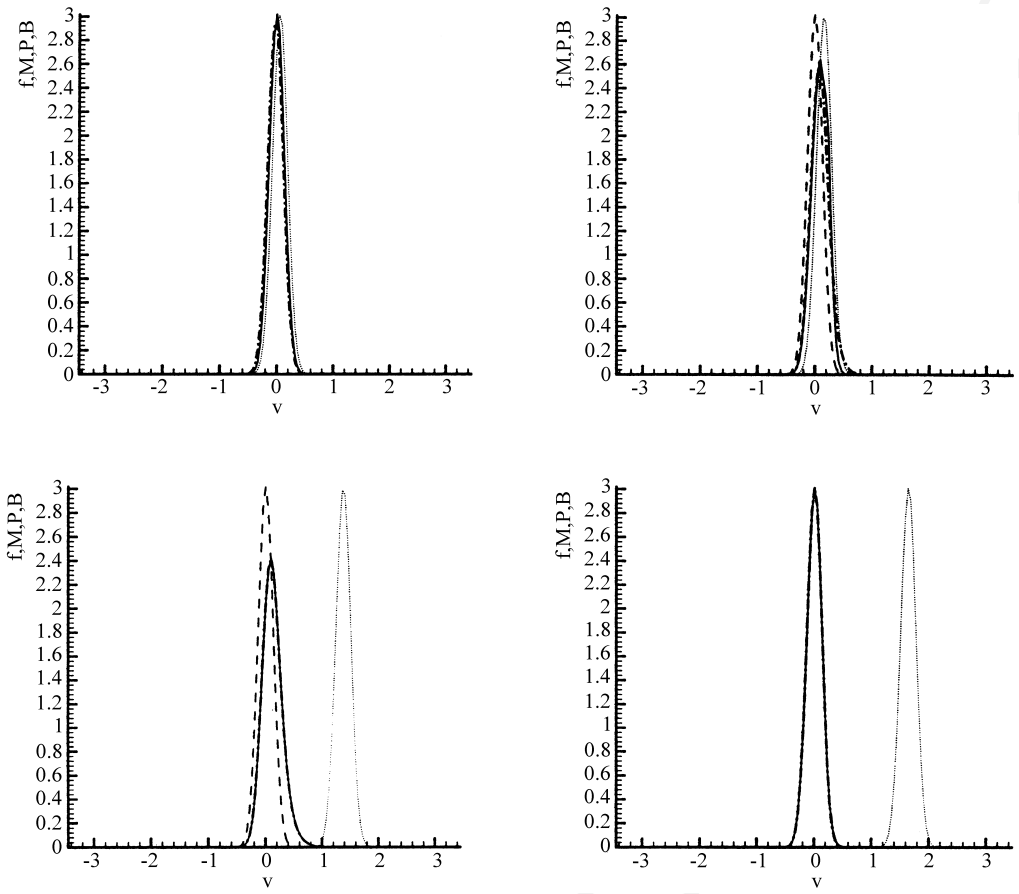

Fig. 2. Normalized stationary distribution $f_\infty(x,v)/\rho_\infty(x)$ at several fixed x for $V_{\text{bias}} = 2\,\text{V}$ for the Si device, obtained from the kinetic simulation and compared to Maxwellians at lattice temperature Θ_0, centered at ballistic velocity and to $P_{-\mu E,\Theta_0}$. Solid line: kinetic solution; dashed line: $M_{\Theta_0}(v)$; dash-dotted line: $P_{-\mu E,\Theta_0}(v)$; dotted line: $B_{\Phi,\Theta_0}(v)$. Top left: at $x = 0.04\,\mu\text{m}$; top right: at $x = 0.12\,\text{mum}$; bottom left: at $x = 0.4\,\mu\text{m}$; bottom right: at $x = 0.52\,\mu\text{m}$.

be time-dependent in the simulation. Typically, one model (Model I) is used in $[0, A]$ and $[B, L]$, another model (Model II) is used in the middle region $[A, B]$. We have the following two methods to deal with the inner boundary conditions at A and B:

- The numerical fluxes $\hat{f}_{j+1/2}$, which are used to compute a conservation approximation to the derivative

$$f_x|_{x=x_j} \approx \frac{1}{\Delta x}(\hat{f}_{j+1/2} - \hat{f}_{j-1/2}),$$

  are computed either by Model I, when the point $x_{j+1/2}$ is inside $[0, A]$ or $[B, L]$, or by Model II, when the point $x_{j+1/2}$ is inside (A, B). This is the standard flux matching procedures used in multi-fluids. Notice that the numerical flux $\hat{f}_{j+1/2}$ involves several neighboring points (the higher the order of accuracy of the scheme, the more neighboring points involved), hence when the point $x_{j+1/2}$ is inside $[0, A]$ but close to the interface A, the computation of the numerical flux $\hat{f}_{j+1/2}$ has already used information from the interval (B, C), even though the flux itself is consistent with that of Model I. The coupling of the two models is thus quite profound. We will refer to this domain decomposition method as the flux matching method.
- Model I is used to compute the solution in the whole interval $[0, L]$. Then, the values of Model I

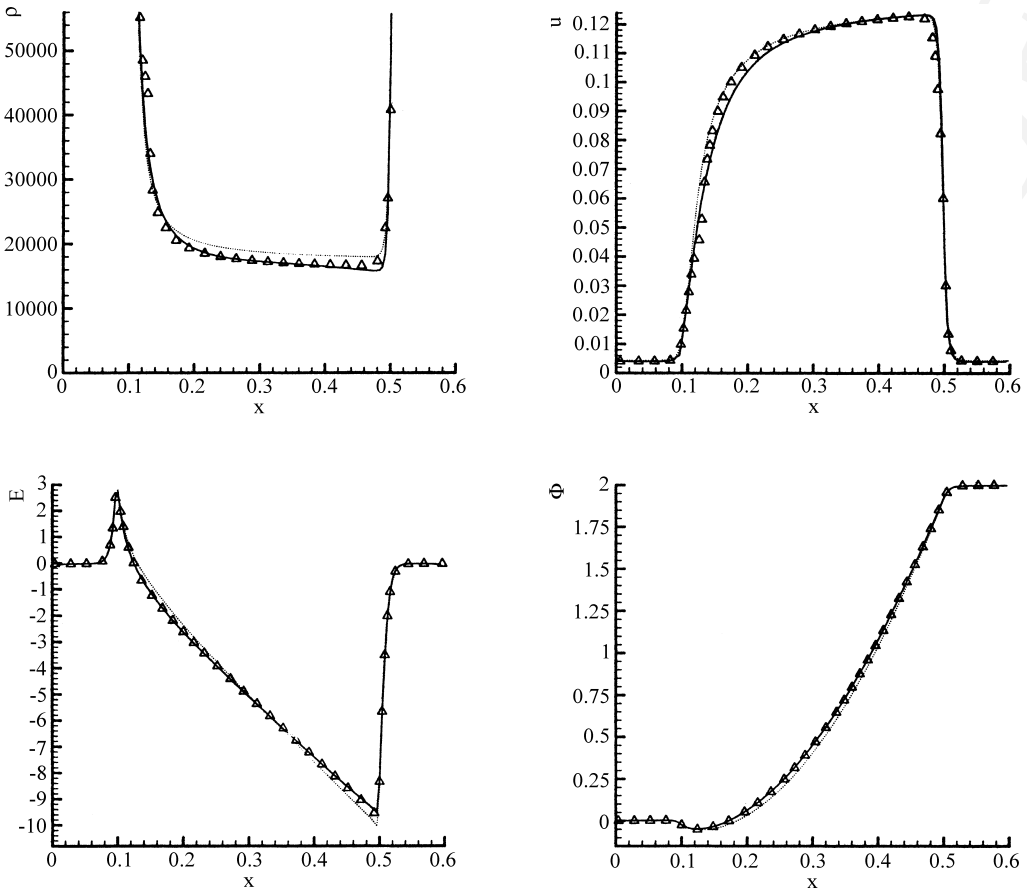

Fig. 3. Numerical comparison of kinetic and drift–diffusion models for the Si n^+–n–n^+ device at $V_{\text{bias}} = 2\,\text{V}$. Solid line: the Boltzmann–Poisson system; dotted line: the DDP system; delta symbols: the domain decomposition LFS–DCBS–LFS flux matching method. Top left: the charge density ρ in μm^{-1}; top right: the (mean) velocity u in μm/ps; bottom left: the electric field E in V/μm; bottom right: the potential Φ in V.

(e.g. concentration ρ and potential Φ) at A and B are used for the boundary condition of Model II in $[A, B]$.

4. Silicon device model

The following silicon device channel simulations provide a computational evidence that the drift–collision balance is achieved within the scale regime given by the silicon device parameters, the channel length and the range of the applied voltages.

Here, we consider a one-dimensional Si n^+–n–n^+ structure of length $L = 0.6\,\mu\text{m}$. The domain of the device is $\Omega = [0, 0.6]$, and the doping profile given by $C(x)$ is a sharp step function with density values $5 \times 10^5 \mu\text{m}$ in $0 \le x \le 0.1$ and in $0.5 \le x \le 0.6$ and $2 \times 10^3 \mu\text{m}$ in $0.1 < x < 0.4$. This is the silicon device analogue of the GaAs device used by Baranger and Wilkins [3]. Our simulations were performed for applied biases V_{bias} from 0 to 3 V, but to save space we shall only include below the results for $V_{\text{bias}} = 2\,\text{V}$.

Other parameters: $m = 0.26 \times 0.9109$ $(10^{-30}\,\text{kg})$, $e = 0.1602$ $(10^{-18}\,\text{C})$, $k_{\text{b}} = 0.138046 \times 10^{-4}$ $(10^{-18}\,\text{J/K})$, $\varepsilon_0 = 11.7 \times 8.85418$ $(10^{-18}\,\text{F}/\mu\text{m})$ and $T_0 = 300\,\text{K}$. Here, we have chosen constant (in x) lattice temperature and variable electron mobility, which are respectively given by $\Theta_0 = (k_{\text{b}}/m)T_0$ and

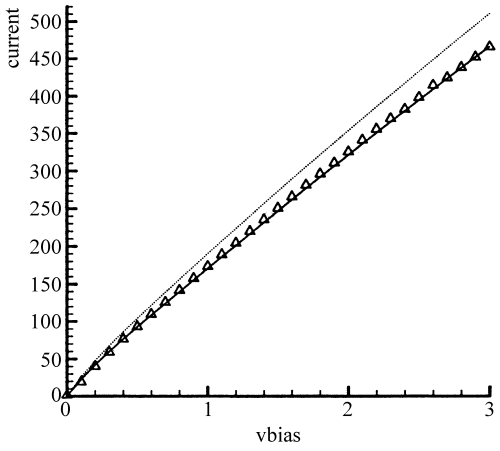

Fig. 4. Current–voltage characteristics for the Si n^+–n–n^+ device. Solid line: the Boltzmann–Poisson system; dotted line: the DDP system; delta symbols: the domain decomposition LFS–DCBS–LFS.

$$\mu(t,x) = \frac{e}{m}\tau(t,x) = \frac{2\mu_0}{1+\sqrt{1+4\left(\frac{\mu_0}{v_d}E(t,x)\right)^2}}, \tag{4.1}$$

where $\mu_0 = 0.1323$ and $v_d = 0.13$.

First we compute the kinetic system (1.1) and (1.2) with the parameters as described above and boundary conditions as described at the end of Section 2. From these computations we identify and plot the non-dimensional parameters $\eta(x), \epsilon(x)$ and $\gamma(x)$ on the left graph and $\alpha(x)$ and $\beta(x)$ on the right graph of Fig. 1. The parameters range of values is characterized by the device specific constants, channel length and applied voltage equals to 2 V.

It is observed that $\eta(x) \simeq 1, \epsilon(x) \simeq 0.05$ inside the channel region, and $\gamma(x)$, though largely varying through the device, is very large in the areas of large doping values and much smaller in the channel region. Since γ is inversely proportional to the characteristic Debye length associated to the non-dimensionalization of the Poisson equation, clearly Debye length asymptotics applied into the system can only be valid in the area of large values of $C(x)$ as it is well known and accepted. In addition, the asymptotics corresponding to the channel region has to be done in the ϵ values for the kinetic self-consistent system.

A point to remark is the fact that the constitutive form of the mobility $\mu(t,x) = \mu(|E|)$ as defined in (4.1), drives all the dimensionless parameters, which involve the field magnitude as well, to be very small varying about constant values $\eta^* = 0.9$, $\epsilon^* = 0.05$ and $\gamma^* = 0.2$ in the channel region, from values of $x = 0.1$ to $x = 0.5\,\mu$m. Thus, according to the asymptotics for the kinetic system introduced in Section 2, this scaling regime of $\eta(x) \simeq 1, \epsilon(x) \ll 1$, or equivalently $\alpha\beta \simeq 0$ and $\alpha/\beta \approx 1$ corresponds to the drift–diffusion balance regime (DCBS), where the moments of the kinetic solution can be approx-

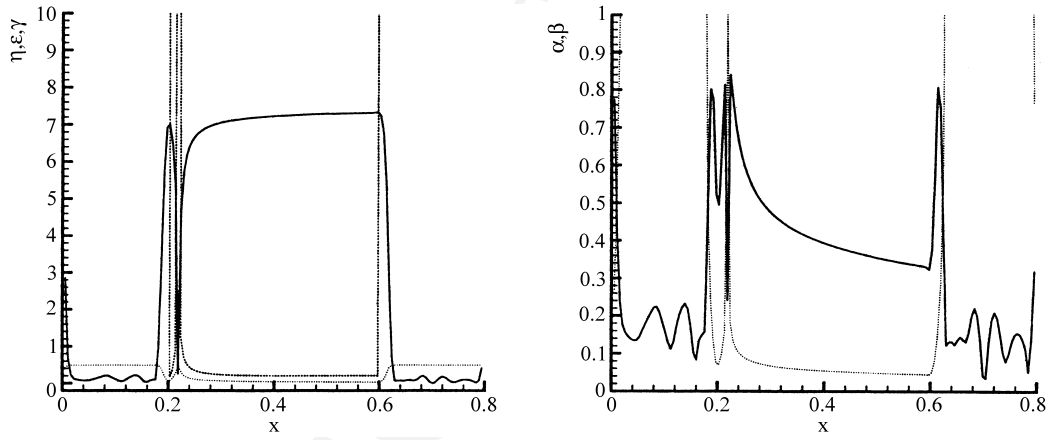

Fig. 5. Local non-dimensional parameters for the GaAs device, calculated with $E(x)$ from the kinetic simulation results. Left figure: solid line, $\eta(x)$; dotted line, $\varepsilon(x)$; dashed line, $\gamma(x)$. Right figure: solid line, $\alpha(x)$; dotted line, $\beta(x)$.

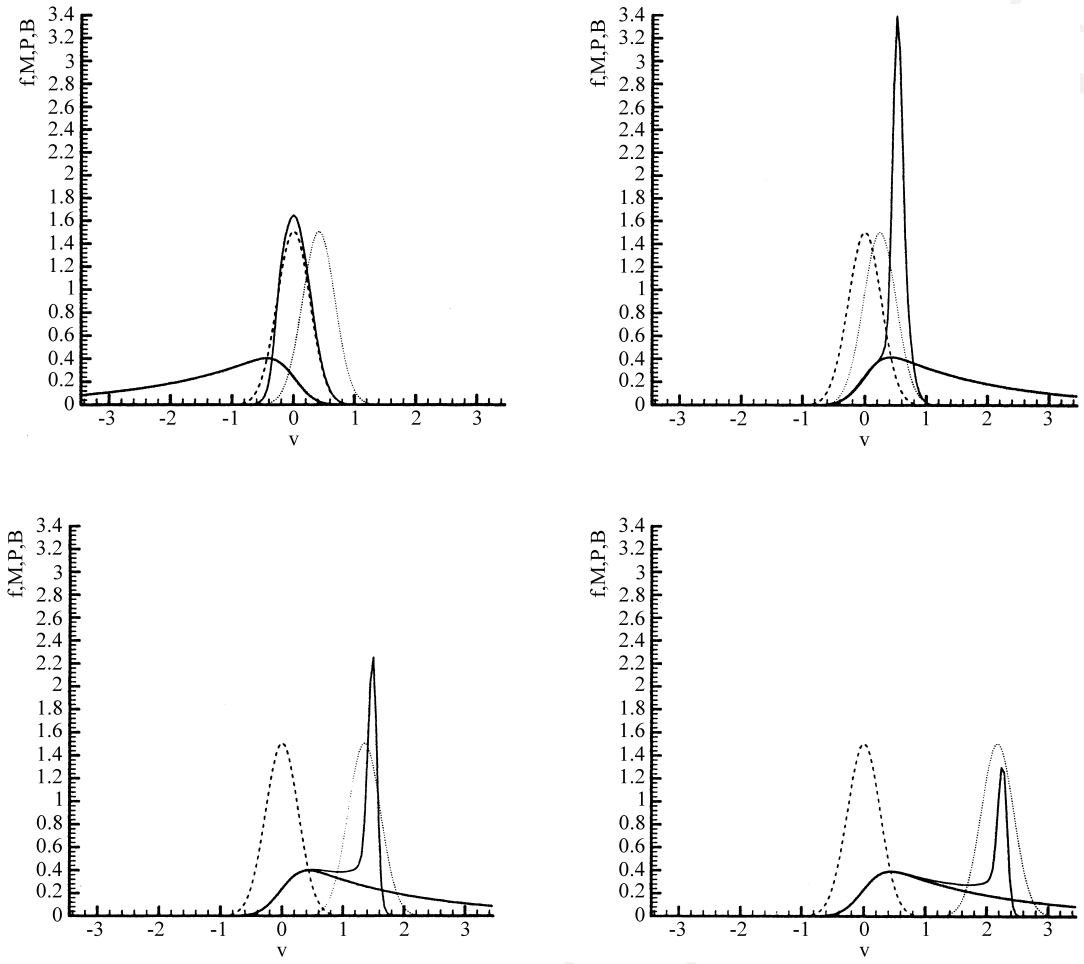

Fig. 6. Normalized stationary distribution $f_\infty(x,v)/\rho_\infty(x)$ at several fixed x for $V_{\text{bias}} = 2\,\text{V}$ for the GaAs device, obtained from the kinetic simulation and compared to Maxwellians at lattice temperature Θ_0, centered at ballistic velocity and to $P_{-\mu E,\Theta_0}$. Solid line: kinetic solution; dashed line: $M_{\Theta_0}(v)$; thick solid line: $P_{-\mu E,\Theta_0}(v)$; dotted line: $B_{\Phi,\Theta_0}(v)$. Top left: at $x = 0.15\,\mu\text{m}$; top right: at $x = 0.2\,\mu\text{m}$; bottom left: at $x = 0.3\,\mu\text{m}$; bottom right: at $x = 0.4\,\mu\text{m}$.

imated by the macroscopic hydrodynamic that solve the ADDP (2.13)–(2.17) times the moments of the solution $P_{-\mu E,\Theta}$ in (2.18) that solves the drift–collision balance equation.

Fig. 2 shows the comparison between the kinetic solution plotted with the Maxwellian centered at zero, the Maxwellian centered at the ballistic speed $B_{\Phi,\Theta_0}(v)$, and the distribution $P_{-\mu E,\Theta_0}$. Though the kinetic solution shows small deviations from $P_{-\mu E,\Theta_0}$ at the channel entrance, as shown for x near 0.1 in the upper right graph of Fig. 2, in the remainder of the channel region, the kinetic solution and $P_{-\mu E,\Theta_0}$ coincide very accurately. In particular, these numerical experiments "validate" the use of the ADDP system when computing macroscopic hydrodynamic variables throughout the channel region.

Therefore, we propose a domain decomposition technique in the space of the dimensionless parameters that involves an adaptive scheme which selects the computation of the DDP equations in highly doped regions and ADDP in the channel region.

Since we notice that the change of scales is driven by the point x^*, where the electrostatic potential reaches its minimum, the one-dimensional domain is cut into

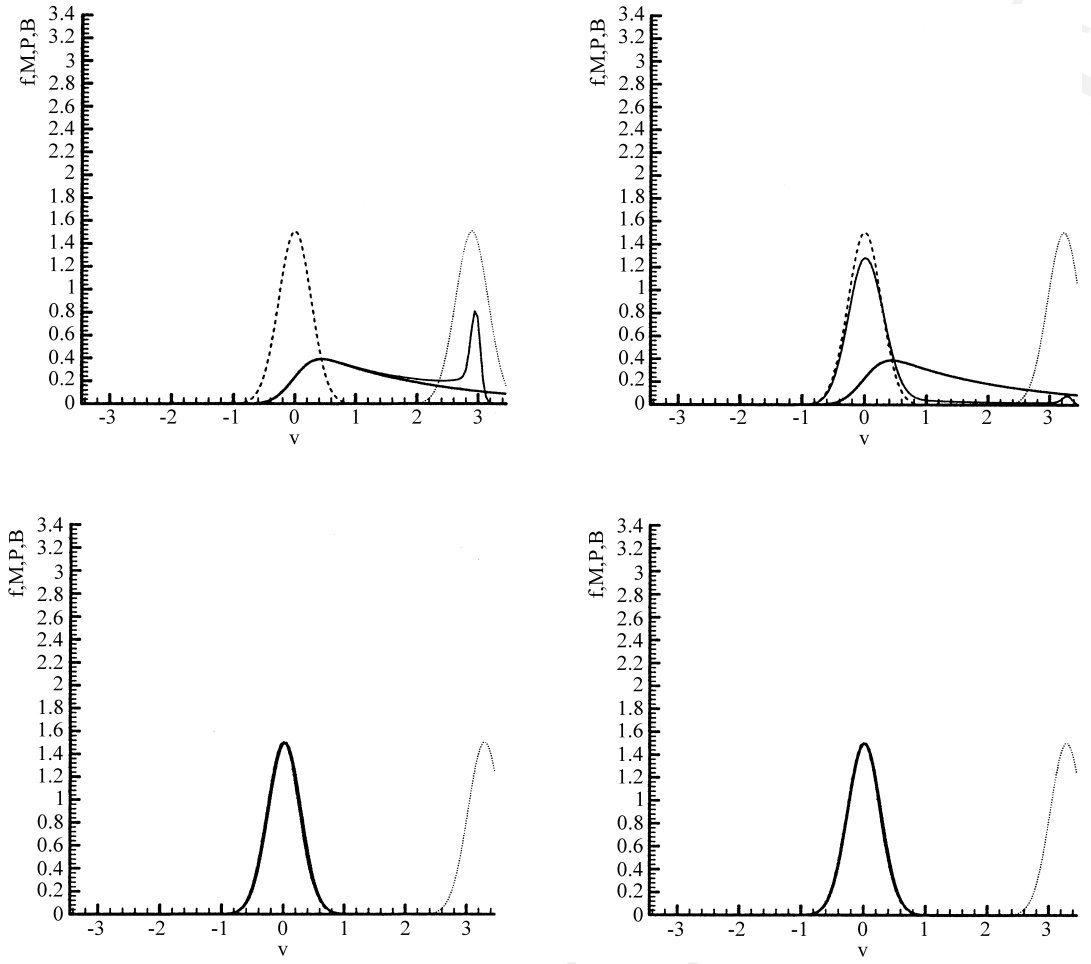

Fig. 7. Normalized stationary distribution $f_\infty(x,v)/\rho_\infty(x)$ at several fixed x for $V_{\text{bias}} = 2\,\text{V}$ for the GaAs device, obtained from the kinetic simulation and compared to Maxwellians at lattice temperature Θ_0, centered at ballistic velocity and to $P_{-\mu E,\Theta_0}$. Solid line: kinetic solution; dashed line: $M_{\Theta_0}(v)$; thick solid line: $P_{-\mu E,\Theta_0}(v)$; dotted line: $B_{\Phi,\Theta_0}(v)$. Top left: at $x = 0.5\,\mu\text{m}$; top right: at $x = 0.55\,\mu\text{m}$; bottom left: at $x = 0.6\,\mu\text{m}$; bottom right: at $x = 0.7\,\mu\text{m}$.

three regions as follows. After choosing a 150 points mesh, a search localizes the mesh point x^*. In order to secure that the scale regime is already the one corresponding to the drift–collision balance one, the change of the computational domain A is chosen at two mesh points on the right of x^*. Notice that this choice of x^*, hence the regions for domain decomposition, is time-dependent and may change each time step. This choice secures that the kinetic system has entered in the scaling regime corresponding to the channel region, where the kinetic solution matches the distribution $P_{-\mu E,\Theta_0}$. The second point B in the domain decomposition is always chosen at the right junction of the doping, where the doping changes from a low value to a high value.

The domain decomposition, shown in Fig. 3, is achieved by the flux matching method between the DDP and the ADDP systems described in the previous section, which is standard in multi-fluid simulations. Our computations show a remarkable improvement with respect to the standard drift–diffusion computations in the whole device.

This type of computation, using WENO schemes, has been already used in [8], however in that work

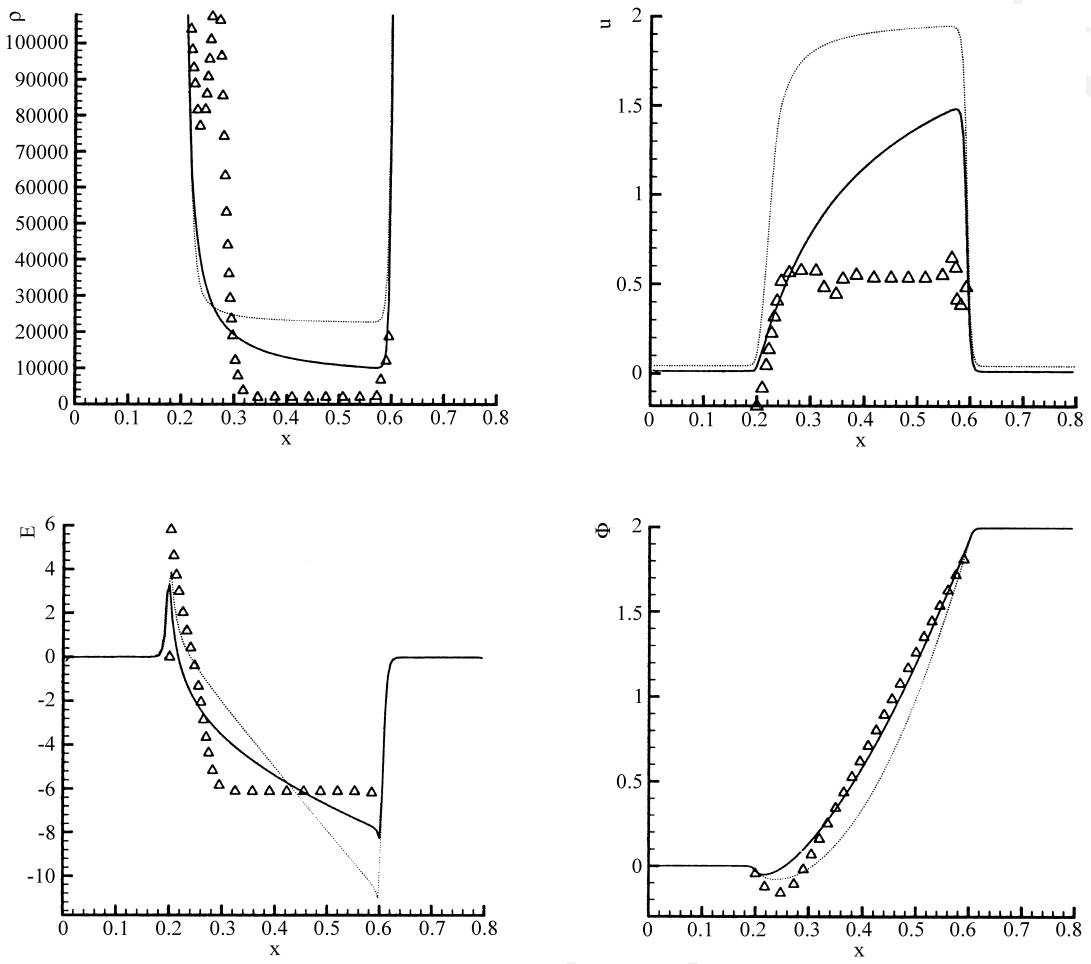

Fig. 8. Numerical comparison of the kinetic, the drift–diffusion model and the HD systems for the GaAs n^+–n–n^+ device at $V_{\text{bias}} = 2\,\text{V}$. Solid line: the Boltzmann–Poisson system; dotted line: the DDP system; delta symbols: the HD system. Top left: the charge density ρ in μm^{-1}; top right: the (mean) velocity u in $\mu\text{m/ps}$; bottom left: the electric field E in $\text{V}/\mu\text{m}$; bottom right: the potential Φ in V.

there was no specific criteria to choose the point x^*, which was obtained basically by trial and error. Here, we have proposed a systematic way of selecting the point x^*. The choice of x_ω in (2.17) is taken at the center of the channel region.

Finally, in Fig. 4 we show three current–voltage characteristic curves. The most deviated from the one produced by the kinetic system is the curve for the DDP system. The IV-curve computed with the domain decomposition shows a sharp improvement (of the order of a factor of 10) over the DDP result. This numerical evidence indicates that the DCBS and thus, the ADDP system, are valid as asymptotic scaling limits for the system (1.1) and (1.2) in this range of parameters.

5. GaAs device model

Here, we consider a one-dimensional GaAs n^+–n–n^+ structure of length $L = 0.8\,\mu\text{m}$. The domain of the device is $\Omega = [0, 0.8]$, and the doping profile given by $C(x)$ is a sharp step function with density values $1 \times 10^6\,\mu\text{m}$ in $0 \le x \le 0.2$ and in $0.6 \le x \le 0.8$ and $2 \times 10^3\,\mu\text{m}$ in $0.2 < x < 0.6$. This

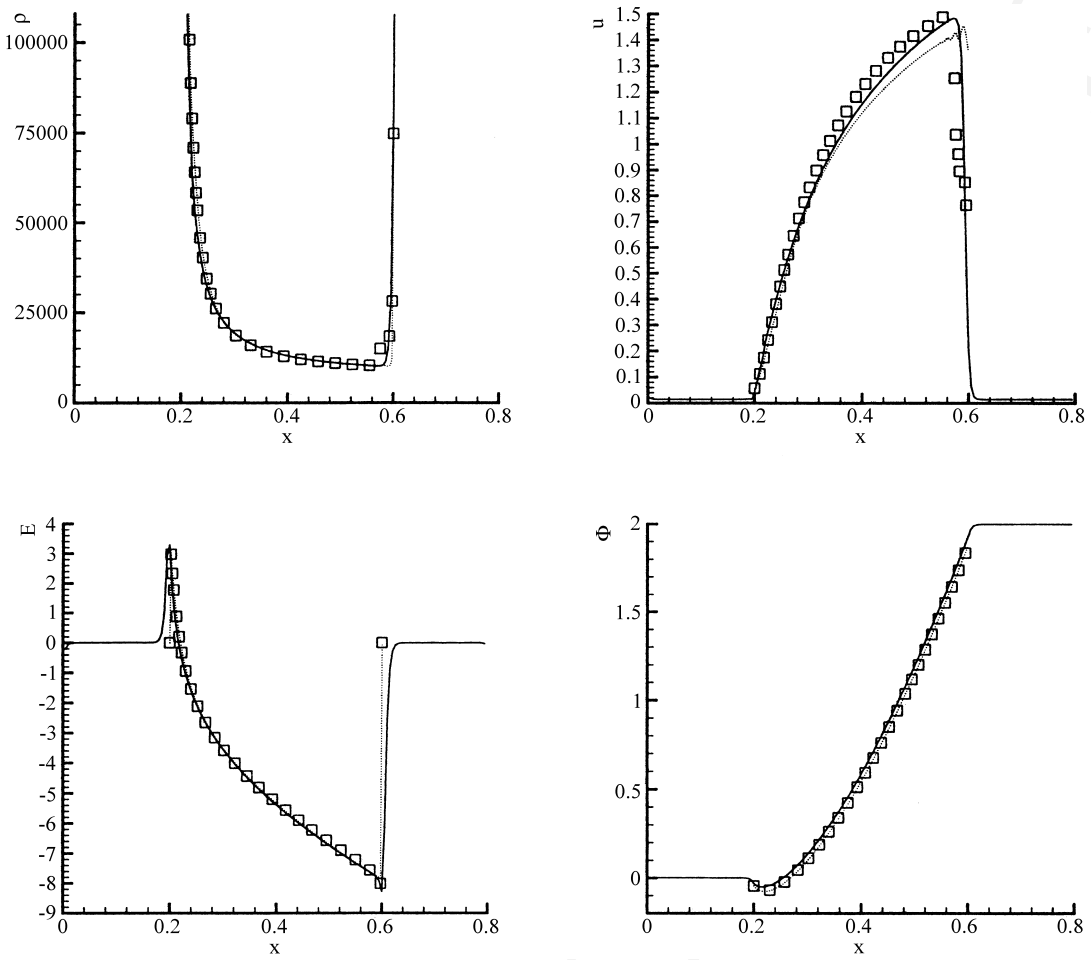

Fig. 9. Numerical comparison of the kinetic and the BHD systems for the GaAs n^+–n–n^+ device at $V_{\text{bias}} = 2\,\text{V}$. Solid line: the Boltzmann–Poisson system; square symbols: the BHDT system; dotted line: the BHD_0 system. Top left: the charge density ρ in μm^{-1}; top right: the (mean) velocity u in $\mu\text{m/ps}$; bottom left: the electric field E in $\text{V}/\mu\text{m}$; bottom right: the potential Φ in V.

is the GaAs device used by Baranger and Wilkins [3,11]. Our simulations were performed for applied biases V_{bias} from 0 to 3 V, but to save space we shall only include below the results for $V_{\text{bias}} = 2\,\text{V}$.

Other parameters: $m = 0.065 \times 0.9109$ $(10^{-30}\,\text{kg})$, $e = 0.1602$ $(10^{-18}\,\text{C})$, $k_{\text{b}} = 0.138046 \times 10^{-4}$ $(10^{-18}$ J/K), $\varepsilon_0 = 13.2 \times 8.85418$ $(10^{-18}\,\text{F}/\mu\text{m})$ and $T_0 = 300\,\text{K}$. The variable electron mobility is given by

$$\mu(t,x) = \frac{e}{m}\tau(t,x) = \frac{2\mu_0}{1+\sqrt{1+4\left(\frac{\mu_0}{v_{\text{d}}}E(t,x)\right)^2}},$$

where $\mu_0 = 4$ and $v_{\text{d}} = 2$.

As in the case of the silicon devices, in Fig. 5 we plot the dimensionless parameters $\eta(x)$, $\varepsilon(x)$ and $\gamma(x)$ on the left-hand side and $\alpha(x)$ and $\beta(x)$ on the right-hand side. The departure from the DCBS is shown by the fact that η is larger than 1 or equivalently, α and β values separate from each other, while β remains very small $\beta \simeq 0.05$. This is the indication of the BS.

Indeed, Figs. 6 and 7 show a comparison of the solution of the kinetic system (1.1) and (1.2) with a Maxwellian centered at zero $M_{\Theta_0}(v)$, a Maxwellian centered at the ballistic speed $B_{\Phi,\Theta_0}(v) = M_{\Theta_0}(v-B)$ and the distribution $P_{-\mu E,\Theta_0}(v)$. Clearly, the kinetic solution cannot be approximated by any of these dis-

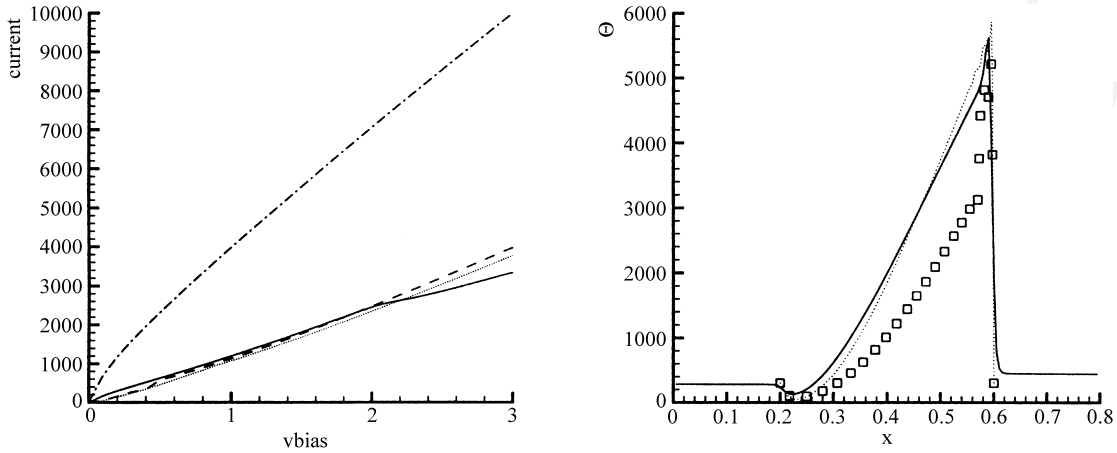

Fig. 10. Left figure: Current–voltage characteristics for the GaAs n^+–n–n^+ device. Solid line: the Boltzmann–Poisson system; dashed line: the BHDT system; dotted line: the BHD_0 system; dash-dotted line: the DDP system. Right figure: numerical comparison of the local temperature for the kinetic and the BHD systems for the GaAs n^+–n–n^+ device at $V_{\text{bias}} = 2\,\text{V}$. Solid line: the Boltzmann–Poisson system; square symbols: the BHDT system; dotted line: the BHD_0 system.

tributions. Nevertheless, well inside the channel, the distribution $P_{-\mu E,\Theta_0}(v)$ captures the tail of the kinetic solution and the distribution $B_{\Phi,\Theta_0}(v)$ localizes the maximum peak of the kinetic solution with a variance that seems to be a fraction of the lattice temperature Θ_0. This observation has led us to the derivation of the hydrodynamic system (2.19), (2.20) and (2.24). This system has been obtained by a moment expansion with the closure based on the ansatz that the kinetic solution is approximated by the convex combination (2.22).

In Fig. 8 we show the comparisons of the kinetic solution, the DDP computation and the hydrodynamic system (HD) used previously in [7,13]. The DDP and the HD results are clearly unsatisfactory. We remark that tests performed in [7] indicate that HD model agrees well with the kinetic calculations when a doping dependent mobility is used, but poorly when a electric field dependent mobility is used, as is done here. We have computed HD only in the channel region [0.2,0.6] with boundary data from the steady results of the DDP computation for the density and the potential, and with temperature boundary condition given by the lattice temperature.

In Fig. 9, we show the comparison between the kinetic, the BHD_0 and the BHDT system. The BHD_0 which corresponds to the pure ballistic case gives us very good results. As a second option, we consider the BHDT system with $\Theta_1 = 0.4\Theta_0$ and ν fixed by the condition (2.23). The choice of the fraction 0.4 is because the variance of the Maxwellian peak of the kinetic distribution function on the channel in Figs. 6 and 7 seems to be of this order. The choice of 0.4 is not important as the results for ν from 0.3 to 0.6 are all similar. The mean velocity is overestimated by the BHDT system while it is underestimated by the BHD_0 system. We have computed BHD_0 and BHDT only in the channel region [0.2,0.6] with boundary data from the steady results of the DDP computation for the density and the potential, and with temperature boundary condition given by the lattice temperature as we did for the HD system.

The codes for BHD_0 and BHDT are extremely stable and run very fast since the CFL condition can be relaxed compared to the HD system, as there is no second derivative heat conduction terms in the system. Comparing computational times, DDP is 10 times faster than BHD_0 or BHDT and the kinetic code is 10 times slower than BHD_0 or BHDT. The computational time for the kinetic run is about 30 min on a Pentium II.

More general domain decomposition for the new hydrodynamic systems BHD_0 or BHDT, perhaps cou-

pled with the original HD, in a way similar to the domain decomposition for DDP and ADDP we performed in the previous section, is currently under investigation and will be reported elsewhere.

The current results in units of $10^{-6}\,\mathrm{A}/\mu\mathrm{m}^2$ for the five runs at $V_{\mathrm{bias}} = 2\,\mathrm{V}$ are summarized in the following table:

Code	Kinetic	DDP	HD	BHD_0	BHD
Current	2394	7062	230	2343	2472

We can clearly see that the DDP system overestimates the current by a tremendous factor while the HD system underestimates it considerably. The comparisons of the current–voltage characteristics for these two systems can be seen in [7].

Next, in Fig. 10 (left-hand side) we have computed the current–voltage characteristics for the kinetic simulation compare to the DDP, the BHD_0 and the BHDT results. The DDP clearly give us very unsatisfactory results. The results of both BHD models are very accurate in general comparing with other known results for this device. For potential drops in the interval [0,0.5] the results are not so good because the transport is not very ballistic for small potential drops. In the interval [0.5,2.0] the model BHDT is a better approximation than the pure ballistic model BHD_0. In the interval [2.0,3.0] BHD_0 is a better approximation than BHDT.

Finally in Fig. 10 (right-hand side) we show the comparisons of the local temperature for the kinetic simulation, the BHDT and the BHD_0 model. The results show that the pure ballistic model gives a better approximation to the temperature than the BHDT model does for $V_{\mathrm{bias}} = 2\,\mathrm{V}$.

6. Conclusions

A numerical study of domain decomposition techniques has been performed and show that charge particle transport in n^+–n–n^+ devices can be very well approximated by a multi-fluid hydrodynamic system of equations. This technique yields considerable better results with respect to drift–diffusion or previous hydrodynamic calculations, at a much lower computational cost than the full kinetic deterministic computations or Monte Carlo computations.

Our computational results show that our technique provides almost identical current–voltage curves as the kinetic ones for dimensions corresponding to a silicon channel device and applied bias between 0.5 and 3 V. In the case of GaAs device dimensions, the improvement is even better, as it is well known that drift–diffusion does not produce good results. The domain decomposition is in the space of the dimensionless parameters, which reflect a delicate interplay between the magnitudes involved.

Acknowledgements

The authors would like to thank A.M. Anile, C. Cercignani and J.W. Jerome for helpful discussions. The first author is supported by the DGESIC MEC-Spain Perfeccionamiento de Doctores en el Extranjero fellowship and the grants ERBFMRXCT970157 (TMR-Network) from the EU and DGES (Spain) PB98-1281. The second author is supported by the National Science Foundation under grant DMS 9971779. The third author is supported by the National Science Foundation under grants ECS-9627849 and ECS-9906606 and by the Army Research Office under grant DAAG55-97-1-0318.

References

[1] A.M. Anile, V. Romano, G. Russo, Extended hydrodynamical model of carrier transport in semiconductors, SIAM J. Appl. Math., in press.
[2] G. Baccarani, M.R. Woderman, An investigation of steady state velocity overshoot effects in Si and GaAs devices, Solid-State Electronics 28 (1985) 407–416.
[3] H.U. Baranger, J.W. Wilkins, Ballistic structure in the electron distribution function of small semiconducting structures: general features and specific trends, Phys. Rev. B 36 (1987) 1487–1502.
[4] N. Ben Abdallah, P. Degond, The Child–Langmuir law for the Boltzmann equation of semiconductors, SIAM J. Math. Anal. 26 (1995) 364–398.
[5] N. Ben Abdallah, P. Degond, A. Yamnahakki, The Child–Langmuir law as a model for electron transport in semiconductors, Solid-State Electronics 39 (1996) 737–744.
[6] K. Blotekjaer, Transport equations for electrons in two-valley semiconductors, IEEE Trans. Electron Devices 17 (1970) 38–47.
[7] C. Cercignani, I.M. Gamba, J.W. Jerome, C.W. Shu, Device benchmark comparisons via kinetic, hydrodynamic, and high-field models, Comput. Meth. Appl. Mech. Eng. 181 (2000) 381–392.

[8] C. Cercignani, I.M. Gamba, J.W. Jerome, C. Shu, A domain decomposition method for Silicon devices, Transport Theory Statist. Phys. 29 (2000) 525–536.
[9] C. Cercignani, I.M. Gamba, C.L. Levermore, A high field approximation to a Boltzmann–Poisson system in bounded domains, Appl. Math. Lett. 4 (1997) 111–118.
[10] C. Cercignani, I.M. Gamba, C.D. Levermore, A drift–collision balance asymptotic to a Boltzmann–Poisson system in bounded domains, Preprint, 1999.
[11] P. Degond, F. Guyot-Delaurens, Particle simulation of the semiconductor Boltzmann equation for one-dimensional inhomogeneous structures, J. Comput. Phys. 90 (1990) 65–97.
[12] H. Grad, Principles of the Kinetic Theory of Gases, Handbuch der Physik (herausgegeben von S. Flgge), Bd. 12, Thermodynamik der Gase. Springer, Berlin, 1958, pp. 205–294.
[13] J.W. Jerome, C.-W. Shu, Energy models for one-carrier transport in semiconductor devices, in: W. Coughran, J. Cole, P. Lloyd, J. White (Eds.), IMA Volumes in Mathematics and Its Applications, Vol. 59, Springer, Berlin, 1994, pp. 185–207.
[14] G. Jiang, C.-W. Shu, Efficient implementation of weighted ENO schemes, J. Comput. Phys. 126 (1996) 202–228.
[15] S.E. Laux, M.V. Fischetti, Transport models for advanced device simulation-truth or consequences? in: Proceedings of the 1995 BCPM, IEEE Electron Devices, 1995, pp. 27–34.
[16] P.A. Markowich, C.A. Ringhofer, C. Schmeiser, Semiconductor Equations, Springer, New York, 1990.
[17] C.A. Ringhofer, Computational methods for semiclassical and quantum transport in semiconductor devices, Acta Numer. 6 (1997) 485–521.
[18] C.-W. Shu, S. Osher, Efficient implementation of essentially non-oscillatory shock capturing schemes II, J. Comput. Phys. 83 (1989) 32–78.
[19] M.S. Shur, L.F. Eastman, Near ballistic transport in GaAs devices at 77 K, Solid-State Electronics 24 (1991) 11–18.